ChemSusChem

Research Article
doi.org/10.1002/cssc.202300385

Chemistry Europe
European Chemical Societies Publishing

www.chemsuschem.org

A Stunt of Sustainability: Artificial Humic Substances Can Generate and Stabilize Single Fe^0 Species on Mineral Surfaces

Fan Yang,*[a, b] Nadezda Tarakina,[c] and Markus Antonietti*[c]

Iron species are omnipresent in fertile soils and contribute to biological and geological redox processes. Here, we show by advanced electron microscopy techniques that an important, but previously not considered iron species, single atom Fe^0 stabilized on clay mineral surfaces, is contained in soils when humic substances are present. As the concentration of neutral iron atoms is highest under frost logged soil conditions, their formation can be attributed to the action of a then reductive microbiome. The Fe^0/Fe^{2+} couple is with −0.04 V standard potential highly suited for natural environmental remediation and detoxification, and its occurrence can help to explain the sustained auto-detoxification of black soils.

Introduction

Humic substances, including humic acids and fulvic acids, are major chemical constituents of the carbon pool in soils. Humic matter plays a number of key roles to sustain soil fertility, such as water binding, ion exchange, phosphate mobilization, and so on.[1] Hardly know to the general scientific public, humins are also a very powerful redox buffer and redox mediator.[2,3] They for instance mediate the extracellular electron transfer within microbial reduction processes, such as iron oxide reduction,[4] thus for instance mediating environmental remediation of perchlorinated biphenyls (PCB).[5] Just recently, the abiotic reduction of silver ions to silver nanoparticles was reported,[6] making silver nanoparticles a potentially naturally occurring species and having impact of the understanding of the geochemistry of trace metals in soils.

The purpose of the present contribution is inspired by these observations but of a more general importance. Iron species are omnipresent in soils, and iron content ranges from 0.2–55 %.[7] Iron content is also known to correlate with carbon degradation in soils,[8] which is understood to be a microbially driven, extracellular, redox mediated process. In freshwater sediments, the interaction of the humic matter redox pool and the iron redox pool was analyzed in more detail,[9] and a dominant role of humic matter shuttling and stabilizing the oxidative/reductive horizons in lake sediments was established. This is usually discussed in relation to the redox process between Fe^{3+}/Fe^{2+} which is located at strongly oxidizing +0.77 V standard potential, but also the Fe^0/Fe^{2+} couple is with −0.04 V in reach of humic matter. Zero-valent Fe nanoparticles (ZVIs) were just recently added to soils for environmental remediation and detoxification[10] and found to be remarkable stable.[11]

It is thereby the target of this contribution to analyze to address the question if natural soils are able to contain and stabilize zero-valent Fe^0 species, appropriate anaerobic conditions assumed. This indeed would represent a natural stunt of sustainable chemistry. As most previous examination excludes the presence of metallic Fe-nanoparticles simply by the absence of the corresponding XRD signals, we will thereby focus on the identification of single Fe^0 species stabilized by the involved mineral surfaces and/or coordinated to humic matter particles. These species can be possibly identified by electron microscopy using electron energy loss spectroscopy (EELS) at the iron core level transitions. Finding such species is highly relevant, as it would point to the natural ability of soils to detoxify themselves in the presence of humic matter, very similar to the technological ZVIs.

The experimental approach is otherwise very simple: we synthesized artificial humic acids (AHA) by a recently described hydrothermal conversion of crude biomass (see Experimental Section) and added it to natural soil. Both the natural and humin-reinforced samples underwent freeze-thaw cycles or not, and the resulting four samples were analyzed for Fe^0.

Results and Discussion

TEM analysis shows that the mineral fraction of all samples consists of two main constituents: SiO_2 and phyllosilicates with up to 5 at.% of Fe. Both phases are easily distinguishable by

[a] Prof. Dr. F. Yang
Joint laboratory of Northeast Agricultural University and Max Planck Institute of Colloids and Interfaces (NEAU-MPICI)
Harbin 150030 (P. R. China)
E-mail: yangfan_neau@163.com
[b] Prof. Dr. F. Yang
School of Water Conservancy and Civil Engineering
Northeast Agricultural University
Harbin 150030 (P. R. China)
[c] Dr. N. Tarakina, Prof. Dr. M. Antonietti
Department of Colloid Chemistry
Max Planck Institute of Colloids and Interfaces
14476 Potsdam (Germany)
E-mail: Markus.Antonietti@mpikg.mpg.de

their morphological appearance in TEM images and in selected area electron diffraction (SAED) patterns, as shown in Figure 1 on artificial humic acid solution (A-HA) containing soil samples.

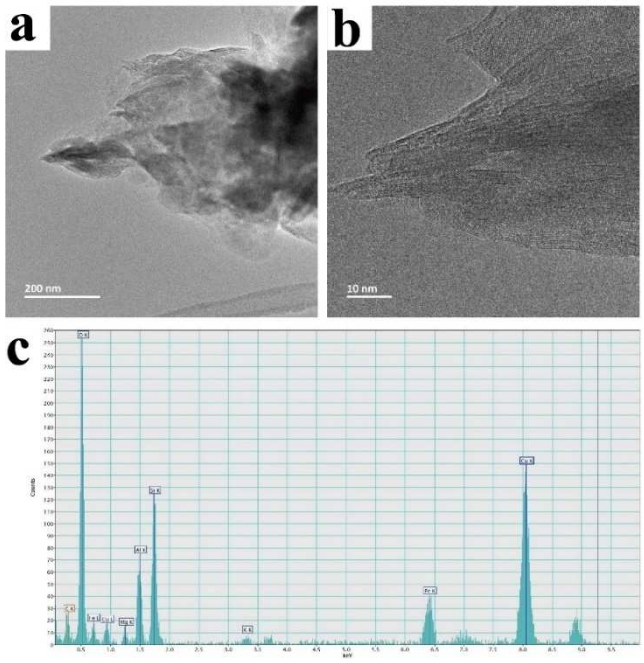

Figure 1. a, b) Two different magnifications of a typical fragment of the soil sample, the higher magnification indicating type and crystallinity of the phyllosilicate mineral fraction. c): Energy dispersive X-ray analysis (EDX) of this spot (intensity in counts over energy in keV) illustrating the presence of alumosilicates, iron, and humic carbon, presumably spread as a disordered layer along the surface of the mineral grains. Cu is from the applied copper grids. EELS has been taken from a variety of similar spots.

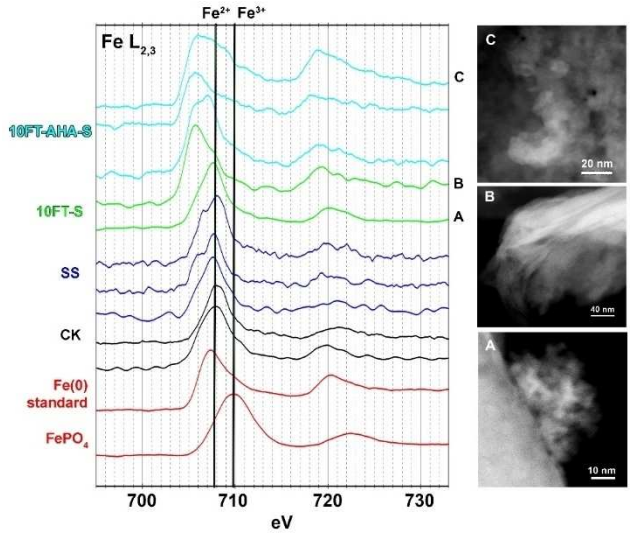

Figure 2. EELS spectra obtained from different soil samples, Fe^0 and $FePO_4$ standards. (a, b) show the typical phyllosilicate area and iron oxide particles from which the spectra of the 10FT–S sample shown on the left (labeled A and B, respectively) have been obtained. (c) HAADF-STEM image of the area in 10FT-AHA–S sample from which the corresponding spectrum marked with C has been collected.

We find overall mostly phyllosilicates, consisting of larger layered flakes mixed with elongated grains, but also smaller fragments of the layered structure. In addition, we find small globular siliciumdioxide particles, mostly quartz. It is important to note that we do not find and analyze larger fragment of biogenic carbon, but that humic matter is mostly found as amorphous surface layers along grains, which are due to contrast reasons hardly visible.

In order to follow the evolution of the oxidation state of iron in different components of the samples (structural Fe in layers of phyllosilicates and Fe in oxidic inclusions, as well as the relevant Fe in the surface carbon layer) a technique that enables determination of elemental composition and oxidation state at high special resolution is required. EELS performed in a scanning transmission electron microscope (STEM) provides this unique combination.[12,13]

Figure 2 shows core-loss EELS spectra collected on differently treated soils, compared to a Fe^0 and a $Fe^{III}PO_4$ standard. The Fe L_3 and L_2 edges are separated by 13 eV, due to 2p spin-orbit coupling, and have similar shapes. One can notice that the reference control group (CK) and sterilized soil of the same type (SS) samples as well as the Fe^0 standard display a similar onset of the core-loss edge at about 705–705.3 eV, however, have different shapes of the edges. Thus, the Fe^0 standard shows the characteristic sharp maximum at 707.4 eV followed by a gradually decreasing shoulder of the peak, which corresponds well to previously reported results on Fe^0, due to the prence of an oxidic surface layer. The $FePO_4$ spectrum has broad peaks at 709.7 eV and 722.5 eV, indicating that Fe in this compound is in oxidation state $3+$.[14,15] The shape of the L_3-edge of the CK sample is typical for Fe^{2+} containing minerals (data not presented here) with an edge maximum at about 707.8 eV and a small shoulder at $\approx$710.5 eV.[15]

For the soil samples, already on sample SS, one starts to notice the appearance of a shoulder at $\approx$706 eV, which becomes even more pronounced in the spectrum of the sample after 10 freeze-thaw cycles (10FT–S) (Figure 2, spectrum A) and starts to dominate in the spectra where both AHA was added and frezze-thaw cycles applied (10FT-AHA-S). The appearance of the shoulder and then the split of the edge with a considerable shift of intensity towards smaller energy values can be explained by the localization of the electrons on the metal. In particular, the shape of the L_3-edge is defined by the weak electron-electron interactions that couple the 2p and 3d electronic states in a single Fe atom. Excitation of a 2p electron to a 3d state leads to a $2p^5 3d^7 4\,s^2$ configuration, giving several possible atomic states, and splitting of the L-edge as has been shown by means of X-ray absorption spectroscopy (XAS) and atomic multiple calculations using the relativistic Hartree–Fock (RHF) approach.[16] A similar explanation can be obtained from crystal-field theory under consideration of a charge transfer. The ligand field surrounding the central metal (Fe) imposes an energy splitting of 3d-orbitals, giving rise to low-spin and high-spin configurations. The 2p electron from the ligand valence band moves to the metal 3d band forming a $3d^7$ configuration with a so-called ligand hole. This transition can considerably increase the electronic density around metal atoms, and thus

the shape of the observed spectral edges, as has been shown by XAS and crystal-field multiplet calculations.[16–18]

Specifically, the use of AHA and applying freeze-thaw cycles considerably increases the localization of electron density at the single Fe-sites, giving rise to the shift of almost 1.5 eV compared to the CK sample. It is worth noticing that a similar shift, of 1.7 eV, was observed by Huse et al. while studying photo-induced spin-state conversion in metal complexes, i.e., it is the sign of electron localization at the iron center, in more simple words a formal reduction.[19]

From the data it is very clear that soil processes can create an electron rich Fe^0 species, or species which are by their redox potential and work function very similar to Fe^0, mostly along the carbon layer on top of the clay mineral. These species are absent in the reference samples, also absent in non-frozen samples (data presentation omitted because of similarity to the reference sample), but show up after freezing and thawing already in natural soil, but are much more pronounced after the addition of artificial humic acid. Formation of the Fe^0 species under freezing conditions can be discussed along recent observations within the metagenomics analysis of such soils.[20] Added humic substances are able to provide unfrozen niches of life even under stronger frost conditions, and metabolic activity continues throughout freezing-thawing cycles. Under such inclusion conditions, the O_2 pool is restricted, and mostly anaerobic processes take place which create a reductive environment. Added humic acid as a then proton-electron "loaded" redox buffer is able to support and stabilize unusual reductive metal species also for longer times and in higher amounts, here Fe^0. This nicely expands recent observations on the abiotic reduction of silver ions to silver nanoparticles by soil organic matter,[6] however to an omnipresent, sustainable, and more powerful reductant, Fe^0, created by anaerobic biological processes.

Conclusion

Redox equilibria are of extreme importance for the sustainability of soils. For the anthropogenic aspects, the removal of industrial pollutants and agrochemicals can proceed both along oxidative and reductive pathways, with the reductive path being usually the weakness of industrial chemicals to attack. The addition of Fe^0 nanoparticles was found to be a powerful, non-toxic countermeasure to attack diverse "anthropogenic supertoxins", such as chlorinated aromatic hydrocarbons, but this treatment comes with expenses and efforts. Here we describe that the addition of artificial humic substances (A-HS) promotes the formation and stability of Fe^0 ad-atoms along the surfaces of layered minerals. A-HS presumably acts in this process as a redox buffer loaded up by anaerobic bacterial operations, in our case supported by frost logging, which reduces the influence of dioxygen. This process also takes place in the reference sample of soils with natural humic acids, however to a significantly lower extent.

These observations partly explain the resilience and chemical self-cleaning of natural black soils via reduction processes, but also open a path a potential tool for a sustainable treatment of polluted industrial soils just by adding A-HA in the presence of a natural soil microbiome. From the view of pure chemistry, it is exciting that single Fe^0 atoms can occur, naturally, in appropriately stabilized polymer surface layers.

Experimental Section

Preparation of soil samples

The original black soil was collected from the layer of soil (0–15 cm) of Xiangyang farm (45°41′ N, 126°37′ E), located in Northeast of China, Harbin. This soil has a poor content of organic matter and organic carbon (0.36%) and was successively air-dried and ground to pass a 2-mm sieve. The other parameters of the original soil are listed in Table 1. Total organic carbon content (TOC) and dissolved organic carbon (DOC) were detected by TOC–L CPN, the content of soil organic matter (SOM) was quantified in a Muffle Furnace (KSL-1100XS), soil electrical conductivity was monitored by a conductivity meter, and the content of cation exchange capacity (CEC) was detected by Kieldahl Azotometer (KjelROC). Additionally, A-HA derived from corn stover was prepared by one-step hydrothermal humification technology (HTH),[21] and TOC content in artificial humic acid solution is as high as $16621 \pm 970\ mg\ L^{-1}$, so the applied liquid addition schemes, i.e., adding a dose of 60 mL, actually translate in an added carbon content of $4986\ mg\ kg^{-1}$ into soil.

Batch soil culture experiments

The investigation is divided into six groups, which were 1) the original soil with 70-day cultivation at room temperature; 2) the original soil after autoclave sterilization at 121 °C for 30 min; 3) the soil after 10 freezing-thawing cycles (70 days); 4) the soil modified by 60 mL A-HA addition with the treatment of 10 freezing-thawing cycles (70 days); 5) the A-HA modified soil added after 70-day cultivation at room temperature; 6) A-HA modified soil with extra 0.10% $FeSO_4 \cdot 7H_2O$ with 70-day cultivation at room temperature. The samples are labelled as CK, SS, 10FT–S, 10FT-AHA–S, AHA–S, AHA–Fe-S.

The soil experiments were performed in pots with 100 mm height and 80 mm. Notably, CK, AHA–S and AHA–Fe-S groups were

Table 1. Parameters of the original soil.

	SOM [%]	TOC [%]	DOC [$mg\ kg^{-1}$]	EC [$\mu s\ cm^{-1}$]	CEC [meq per 100 g]
CK	5.76	0.36	868.5	63.40	15.60
SS	5.88	0.42	772.0	82.50	16.22
10FT-S	6.40	0.36	1119.80	43.97	18.02
10FT-AHA-S	6.05	0.79	1985.53	368.33	15.30
AHA-S	6.30	0.62	1240.20	100.30	15.85
AHA–Fe-S	6.11	0.59	1155.41	138.20	16.26

conducted in an incubator at constant 25 °C, and 10FT–S and 10FT-AHA–S groups were placed in a freezing-thawing cycle apparatus where a single cycle was set at −15 °C for 2 days and 10 °C for 5 days, that is, the treatment of10 freezing-thawing cycles takes 70 days.

To reduce the evaporation of water and block germination from the outside environment without affecting the respiration of the soil, specially, the top of each pot was covered with a layer of breathable sealing film. CK, AHA–S and AHA–Fe-S groups were sprayed with distilled water every 7 days to maintain constant water content, and 10FT–S and 10FT-AHA–S groups were sprayed with distilled water at the end of each freezing-thawing cycle.

TEM-EELS analyses

For scanning transmission electron microscopy (STEM) observations, a suspension of the sample in ethanol was sonicated for 5–10 min and then drop-casted to the Cu grid with a lacey carbon support and dried for 10 min. The STEM study was performed using a double Cs corrected JEOL JEM-ARM200F (S)TEM operated at 80 kV and equipped with a cold-field emission gun and a high-angle silicon drift EDX detector (solid angle up to 0.98 steradians with a detection area of 100 mm^2). Annular dark field scanning transmission electron microscopy (ADF-STEM) images and EELS spectra were collected at a probe convergence semi-angle of 25 mrad. EELS spectra from all samples and standards were recorded in dual EELS mode at energy dispersions 0.1 $eV\,ch^{-1}$ and 0.25 $eV\,ch^{-1}$, allowing correction for the zero-loss peak position. The Power law model was used for the background subtraction. Multiple scattering effects have been removed using the Fourier ratio method, implemented in the Gatan Digital micrograph suit. The numerical smooth filer (low-pass parameter 1.0) has been applied to all spectra.

Acknowledgements

The authors like to thank the continued support of the Max Planck Society. Fan Yang acknowledges the funding from the Outstanding Youth Project of Heilongjiang Province (JQ2021D001) and the support by the Outstanding Young Talents Project (2020YQ14) as a Youth Longjiang Scholar. Open Access funding enabled and organized by Projekt DEAL.

Conflict of Interests

The authors declare no conflict of interest.

Data Availability Statement

The data that support the findings of this study are available from the corresponding author upon reasonable request.

Keywords: soil chemistry · detoxification · artificial humic acid · single atom catalysis · Fe^0 remediation

[1] F. Yang, C. Y. Tang, M. Antonietti, *Chem. Soc. Rev.* **2021**, *50*, 6221–6239.
[2] C. F. Zhang, A. Katayama, *Environ. Sci. Technol.* **2012**, *46*, 6575–6583.
[3] C. F. Zhang, S. H. You, H. Y. Dang, Z. L. Li, Q. L. Xie, D. D. Zhang, *J. Soils Sediments* **2019**, *19*, 2594–2603.
[4] E. J. A. Smith, P. L. Tremblay, P. M. Shrestha, O. L. Snoeyenbos-West, A. E. Franks, K. P. Nevin, D. R. Lovley, *Nat. Geosci.* **2010**, *3*, 417–421.
[5] D. D. Zhang, H. Y. Dang, Z. L. Li, C. F. Zhang, *Environ. Pollut.* **2019**, *252*, 296–304.
[6] Y. N. Huang, T. T. Qian, F. Dang, Y. G. Yin, M. Li, D. M. Zhou, *Nat. Commun.* **2019**, *10*, 8.
[7] I. Bodek, W. J. Lyman, W. F. Reehl, *Environmental Inorganic Chemistry*, Pergamon Press, New York, **1988**, pp. 16–17.
[8] W. Emsens, C. J. S. Aggenbach, K. Schoutens, A. J. P. Smolders, D. Zak, R. van Diggelen, *PLoS One* **2016**, *11*, 17.
[9] A. Kappler, M. Benz, B. Schink, A. Brune, *FEMS Microbiol. Ecol.* **2004**, *47*, 85–92.
[10] Y. Z. Liu, T. Wu, J. C. White, D. H. Lin, *Nat. Nanotechnol.* **2021**, *16*, 197–205.
[11] Q. Du, G. X. Li, S. S. Zhang, J. P. Song, Y. Zhao, F. Yang, *J. Hazard. Mater.* **2020**, *383*, 9.
[12] L. A. J. Garvie, P. R. Buseck, *Nature* **1998**, *396*, 667–670.
[13] L. A. Grunes, R. D. Leapman, C. N. Wilker, R. Hoffmann, A. B. Kunz, *Phys. Rev. B* **1982**, *25*, 7157–7173.
[14] A. Augustsson, G. V. Zhuang, S. M. Butorin, J. M. Osorio-Guillen, C. L. Dong, R. Ahuja, C. L. Chang, P. N. Ross, J. Nordgren, J. H. Guo, *J. Chem. Phys.* **2005**, *123*, 184717.
[15] L. A. J. Garvie, A. J. Craven, R. Brydson, *Am. Miner.* **1994**, *79*, 411–425.
[16] P. S. Miedema, F. M. F. de Groot, *J. Electron Spectrosc. Relat. Phenom.* **2013**, *187*, 32–48.
[17] E. C. Wasinger, F. M. F. de Groot, B. Hedman, K. O. Hodgson, E. I. Solomon, *J. Am. Chem. Soc.* **2003**, *125*, 12894–12906.
[18] P. Gambardella, S. S. Dhesi, S. Gardonio, C. Grazioli, P. Ohresser, C. Carbone, *Phys. Rev. Lett.* **2002**, *88*, 4.
[19] N. Huse, T. K. Kim, L. Jamula, J. K. McCusker, F. M. F. de Groot, R. W. Schoenlein, *J. Am. Chem. Soc.* **2010**, *132*, 6809–6816.
[20] C. Y. Tang, B. L. Liu, K. Cheng, M. Antonietti, F. Yang, *Land Degrad. Dev.* **2023**, *34*, 1352.
[21] F. Yang, S. S. Zhang, K. Cheng, M. Antonietti, *Sci. Total Environ.* **2019**, *686*, 1140–1151.

Manuscript received: March 22, 2023
Revised manuscript received: March 31, 2023
Accepted manuscript online: April 3, 2023
Version of record online: June 16, 2023